Monthly Notices
of the
ROYAL ASTRONOMICAL SOCIETY

MNRAS **472,** 3833–3841 (2017)
Advance Access publication 2017 August 24

doi:10.1093/mnras/stx2175

A two-population sporadic meteoroid bulk density distribution and its implications for environment models

Althea V. Moorhead,[1]★ Rhiannon C. Blaauw,[2] Danielle E. Moser,[3]
Margaret D. Campbell-Brown,[4] Peter G. Brown[4] and William J. Cooke[1]

[1]*NASA Meteoroid Environment Office, Marshall Space Flight Center, Huntsville, AL 35812, USA*
[2]*All Points Logistics, Jacobs ESSSA Group, Marshall Space Flight Center, Huntsville, AL 35812, USA*
[3]*Jacobs, ESSSA Group, Marshall Space Flight Center, Huntsville, AL 35812, USA*
[4]*Department of Physics and Astronomy, The University of Western Ontario, London N6A3K7, Canada*

Accepted 2017 August 22. Received 2017 August 15; in original form 2016 November 30

ABSTRACT

The bulk density of a meteoroid affects its dynamics in space, its ablation in the atmosphere, and the damage it does to spacecraft and lunar or planetary surfaces. Meteoroid bulk densities are also notoriously difficult to measure, and we are typically forced to assume a density or attempt to measure it via a proxy. In this paper, we construct a density distribution for sporadic meteoroids based on existing density measurements. We considered two possible proxies for density: the K_B parameter introduced by Ceplecha and Tisserand parameter, T_J. Although K_B is frequently cited as a proxy for meteoroid material properties, we find that it is poorly correlated with ablation-model-derived densities. We therefore follow the example of Kikwaya et al. in associating density with the Tisserand parameter. We fit two density distributions to meteoroids originating from Halley-type comets ($T_J < 2$) and those originating from all other parent bodies ($T_J > 2$); the resulting two-population density distribution is the most detailed sporadic meteoroid density distribution justified by the available data. Finally, we discuss the implications for meteoroid environment models and spacecraft risk assessments. We find that correcting for density increases the fraction of meteoroid-induced spacecraft damage produced by the helion/antihelion source.

Key words: meteorites, meteors, meteoroids.

1 INTRODUCTION

The density of a meteoroid is a critical quantity that reflects the origin of a particle and influences its dynamical behaviour and its response to collision. Density can serve as a clue to meteoroid composition and potentially strengthen or weaken the case for a particular origin scenario. Once liberated from its parent, a meteoroid in space is subjected to radiation pressure and Poynting–Robertson drag, both of which will be proportionally weaker per unit mass for a denser meteoroid. When a meteoroid enters the atmosphere, a lower density will result in both greater deceleration and more rapid ablation.

Bulk density also factors into spacecraft risk assessments. The damage incurred on spacecraft surfaces by debris is a function of projectile mass, speed, impact angle and density [see the ballistic limit equation (BLE) discussion in Section 6]. Environment models such as NASA's Meteoroid Engineering Model (MEM; McNamara et al. 2004) report meteoroid fluxes to a limiting mass and pair these fluxes with directionality and speed information. The density distribution of these models, however, tends to be far less detailed than that of directionality and speed; this is due to the difficulty of measuring meteoroid bulk densities and the corresponding lack of data.

As an example, MEM currently uses a single meteoroid density of 1000 kg m^{-3}. NASA's previous model, described in TM-4527, used a step function in which a different density value was used for each of three mass ranges. The frequently used meteoroid mass distribution of Grün et al. (1985) was derived assuming a constant density of 2500 kg m^{-3}. None of these is particularly realistic; natural meteoroids are likely to have a distribution of densities. The incorporation of such a distribution is a key goal for the next version of MEM and prompts us to take a fresh look at the meteoroid density distribution.

In addition to damaging spacecraft surfaces, meteoroids create microcraters on natural surfaces (e.g. lunar rocks) that are not protected by an atmosphere. The depth-to-diameter ratios of microcraters have been argued to be a strong proxy for the impactor bulk

★ E-mail: althea.moorhead@nasa.gov

density (Leinert & Grün 1990), though velocity also likely plays a role. As summarized in D'Hendecourt & Lamy (1980), the microcrater data suggest that larger particles (from several μm up to ≈100 μm) are silicate-type density. There is less evidence for a predominance of very low bulk density meteoroids based on the microcratering data alone, a conclusion also supported by Helios data (Grün et al. 1980), although the latter data correspond only to particles smaller than a few μm.

While the non-destructive capture of evolved, macroscopic meteoroids has not yet been accomplished, interplanetary dust particles (IDPs) have been collected in the stratosphere (e.g. Messenger et al. 2015) and recently ejected particles have been collected near comets (e.g. Brownlee et al. 2006). One recent example of the latter is the collection of mm-sized dust grains from comet 67P/Churyumov-Gerasimenko by the Grain Impact Analyzer and Dust Accumulator (GIADA) instrument on Rosetta (Fulle et al. 2015) and direct characterization of sub-mm grains by the COSIMA instrument (Hornung et al. 2016). GIADA collected more than 300 dust particles ejected by the comet, which fell into two broad categories: compact grains and fluffy aggregates. Densities ranged from 800 to 3000 kg m^{-3}, and the particles are approximately mm-sized, placing them in our mass range of interest (i.e. particles large enough to damage spacecraft surfaces). This indicates that particles ejected from the same comet have a range of bulk densities. However, these are freshly ejected particles whose material properties could change over time due to sublimation of volatiles, collisions or irradiation. Such a model was proposed by Mukai & Fechtig (1983), who showed that meteoroid bulk densities would be expected to increase over time due to solar heating. As another example, Borovička (2007) cites solar heating as altering the properties of Geminid meteoroids, which are fairly dense. Sporadic meteoroids will in general be older and resemble cometary ejecta even less than shower meteoroids.

Direct measurement of bulk densities of IDPs captured in the stratosphere may also provide some constraints on meteoroid bulk densities. However, this sample is heavily biased towards slow, small particles (Flynn 1990); in most cases, the measured bulk densities are for particles too small to pose a hazard to spacecraft (100-μm-and-larger particles). Furthermore, interaction with the atmosphere may alter bulk density, making it likely that exoatmospheric particles are less dense than stratospherically measured IDPs (Flynn 1994). With these caveats in mind, a compilation of all IDP (sizes from 6 to 30 μm) bulk density measurements by Flynn & Sutton (1991) showed a bimodal distribution with a low-density peak near 600 kg m^{-3} and a higher density peak near 2000 kg m^{-3}. More recent work (Kohout et al. 2014) shows higher densities for some micrometeorites (up to 5700 kg m^{-3}) and emphasizes the role of atmospheric heating in modifying porosity and bulk density.

One could also attempt to extrapolate a meteoroid bulk density distribution from comets and asteroids, from which meteoroids originate. However, cavities and macroporosity in these larger objects can cause a mismatch in density between meteoroids and their parent bodies. Meteorites are often denser than asteroids, and macroporosity is known to exist in comets as well as asteroids (Carry 2012). For this reason, we also discard the parent body approach to determine meteoroid densities.

Due to the limitations of the above approaches and our need to correlate orbital parameters with meteoroid bulk densities in developing any generalized model, we rely primarily on meteor ablation models to constrain density. These models work as follows: if a meteoroid exhibits measurable deceleration, the physical quantities (or combinations of physical quantities) of the meteoroid can be constrained by simultaneously reproducing its deceleration and light emission. A number of authors have used this approach to constrain density (Ceplecha 1977; Revelle 1983, 2001; Bellot Rubio et al. 2002; Borovička, Spurný & Koten 2007); Section 2 briefly reviews recent advances in ablation modelling.

For many data sets, this type of detailed ablation modelling is often not possible. The NASA All Sky Fireball Network (Cooke & Moser 2012), for instance, does not observe meteors with fine enough resolution to constrain densities well. Transverse scattering radars such as the Canadian Meteor Orbit Radar (CMOR; Campbell-Brown 2008) can detect millions of meteors, but even with half a dozen receiver stations only a few points along the trajectory have measurable ionization, making ablation modelling largely unconstrained. A valid proxy for density would nevertheless allow us to incorporate bulk densities into the analysis of these data sets, and the purpose of this work is to select such a proxy.

In Section 2, we review works that constrain meteoroid densities using ablation modelling and therefore provide us with opportunities to explore density proxies. In Section 3, we assess the degree to which density is correlated with the K_B parameter using trajectory and density information provided by Kikwaya et al. (2011) and Campbell-Brown et al. (2013). In Section 4, we consider the relationship between density and the Tisserand parameter noted by Kikwaya et al. (2011) using values from Kikwaya et al. (2009, 2011) and Campbell-Brown et al. (2013) and compare it with the correlation between density and K_B. In Section 5, we develop a two-population density model from these data. Finally, Section 6 presents the impact that this model has on the near-Earth meteoroid environment encountered by spacecraft.

2 DENSITY MEASUREMENTS FROM ABLATION MODELLING

Meteor ablation modelling is more than 60 years old (see e.g. Opik 1958), but we restrict our review to recent advances in meteor ablation modelling (a review of older literature is available in Borovička 2006, 2007).

Over time, ablation models have increased in complexity in attempts to explain observed features. For instance, early models focused on single-body (non-fragmenting) solutions. In general, it is widely observed that meteoroids at all sizes fragment, so ignoring fragmentation in ablation modelling leads to systematic biases. Fragmentation must be included in order to explain variable light-curve shapes and spikes in brightness; excluding fragmentation can lead to overly large ablation coefficients and density underestimates (as seen in Bellot Rubio et al. 2002). At fireball sizes, fragmentation has historically led to a large discrepancy between photometric masses (determined from light curves) and dynamic masses (measured from deceleration). Ceplecha & ReVelle (2005) demonstrated that fragmentation was the root cause of this problem, producing larger apparent ablation coefficients and luminous efficiencies. Similarly, while earlier works such as Babadzhanov (2002) derived densities using only the light curve, the more recent models discussed in this section also make use of the meteoroid's dynamics to constrain meteoroid properties.

Drew et al. (2004) conducted a meteoroid density survey based on ablation modelling, using 572 radar meteor head echoes obtained from ALTAIR (over 900 were later analysed in Drew 2005). Their model allowed for fragmentation only through the use of a 'parameter of shape variation'. Although they derived densities for a large set of meteoroids their data were biased heavily towards apex meteoroids. A more sophisticated version of this study was presented

by Close et al. (2012), who used an expanded model to estimate dynamic mass and improved radar signal processing to increase the quality of the measured head echoes. Both of these radar studies found representative bulk densities for apex meteoroids near 900 kg m^{-3}, appropriate to meteoroids with typical masses of 10^{-7} to 10^{-8} kg corresponding to diameters of the order of several hundred μm.

Borovička et al. (2007) described a 'thermal erosion' ablation model in which grains continually detach from the main meteoroid mass. This model was used to estimate the bulk density of seven Draconid meteoroids. Density was degenerate with grain shape, but the author used a shape parameter intermediate to that of a disc and a sphere to obtain a meteoroid bulk density of 300 kg m^{-3} for the Draconids. Although this is one of the best ablation models currently available, the Draconids themselves are not a good stand-in for sporadic meteoroids. Borovička et al. (2007) agreed with Jacchia, Kopal & Millman (1950) that Draconids have higher starting and ending heights than sporadic meteors with the same velocity, indicating that they most likely have different material properties. For this reason, we exclude these measurements from our sporadic density model.

Campbell-Brown & Koschny (2004) described a 'thermal disruption' ablation model in which the constituent components of small meteoroids are released simultaneously at the onset of ablation. Kikwaya et al. (2009) applied this model to a set of 42 optical double-station meteors and were able to obtain densities for six of them. Kikwaya et al. (2011) applied the same method to a set of more than 100 meteors (92 successfully), including both sporadic and shower meteors, with a wide range of speeds. A notable feature of Kikwaya et al. (2009, 2011) is that the authors systematically searched their parameter space for chi-squared minima before refining their fits. They often found multiple chi-squared minima for significantly different values of density, from which they selected the global minimum to refine. This indicates that studies that do not conduct this search could obtain densities corresponding to local, but not global, chi-square minima, producing 'best-fitting' densities that are considerably off from the true best fit.

Campbell-Brown et al. (2013) applied both the thermal disruption ablation model of Campbell-Brown & Koschny (2004) and the thermal erosion ablation model of Borovička et al. (2007) to 10 precisely tracked meteors, seven of which are sporadic, and compare the results. The light curve and deceleration were used to constrain meteor properties; the models were then judged by their ability to correctly reproduce the light curve, deceleration and meteor train. The thermal erosion model of Borovička et al. (2007) was deemed to be more successful in reproducing the shape of the light curve at the beginning of the event and the deceleration at the end. However, it also tended to overpredict the length of meteor wakes. The paper thus demonstrated that two of the most state-of-the-art meteor ablation models struggle to reproduce all observed meteor features.

Our goal is to extrapolate a sporadic meteoroid bulk density distribution from the set of existing meteoroid bulk densities that have been constrained by ablation modelling. Ideally, the studies used [1] include the effects of fragmentation in their ablation model(s) and [2] fully explore the parameter space to determine the best density solution. We also prefer that the data [3] consist primarily of sporadic meteoroids, [4] contain representatives from each sporadic source and [5] lie within the 'threat regime' (ideally between 1 μg and 1 mg; more massive meteoroids are of course also hazardous but are much less numerous). Three of the works discussed in this section meet all or most of our criteria. Kikwaya et al. (2009, 2011) meet all five criteria; Campbell-Brown et al. (2013) meet all but criterion 2 (full exploration of the parameter space). In the following sections, we use the results of these three studies to examine density proxies and construct a density model that is appropriate for environment models such as MEM.

3 CORRELATION WITH K_B

Using the expression originally derived by Levin (1956) for the temperature at the surface of a meteoroid, Ceplecha (1958) proposed an equation relating the physical properties of a meteoroid to a single parameter representing its strength:

$$K_B = \log \rho_B + \frac{5}{2} \log v_\infty - \frac{1}{2} \log \cos z_R \qquad (1)$$
$$= \log \frac{2\tau_B}{a} + \frac{1}{2} \log \lambda \delta c b.$$

The quantities on the top line are observable quantities: ρ_B is the air density (in g cm^{-3}) at which ablation begins, v_∞ is the original velocity in cm s^{-1} and z_R is the zenith distance of the radiant. Meteoroid material properties are relegated to the lower line; τ_B is the surface temperature at which ablation begins, a is the accommodation coefficient, λ is heat conductivity, δ is meteoroid bulk density and c is specific heat. Measurable quantities such as meteor start height, velocity and zenith angle thus effectively measure a combination of meteoroid material properties. The remaining quantity, b, represents the inverse of the air density scaleheight. While it is arguably an 'observable quantity', it varies very little in comparison with air density and velocity, and is thus typically bundled together with material properties and ignored.

Ceplecha applied K_B to a total of 217 meteors published in Jacchia (1952) and from Ondrejov, the parameters for which are replicated in Ceplecha (1958). The result was a double-peaked histogram, which Ceplecha used to divide the data into two populations. In later works, Ceplecha divided meteors into additional populations (A, B, C and asteroidal) with less-obvious divisions (Ceplecha 1966a, 1967, 1977). These were also further divided into subpopulations (C1, C2 and C3) based on semi-major axis and inclination (Ceplecha 1967). This classification is often referred to as 'Ceplecha type'.

Ceplecha also attempted to correlate these populations with densities (Ceplecha 1966b). Specifically, he found a correlation between K_B and the ratio of photometric to dynamic mass. Although Ceplecha notes the degeneracy among meteoroid bulk density, drag coefficient, shape factor and optical depth, he nevertheless associates a density with each K_B class. He initially associated a density of 4000 kg m^{-3} with A-type meteoroids, 2200 kg m^{-3} with B-types and 1400 kg m^{-3} with C-types (these values were revised downward in subsequent works.). A type D was later added to describe soft cometary material with a density estimated at 270 kg m^{-3} (Ceplecha 1988). Many subsequent studies continued to associate densities or density ranges with Ceplecha types (Ceplecha 1977; Revelle 1983, 2001; Ceplecha et al. 1998; Bellot Rubio et al. 2002; Kikwaya et al. 2011).

As discussed in Section 2, ablation models have become substantially more detailed over time as computing power has increased, and the most recent models now include effects such as fragmentation. We re-investigate the correlation between density and Ceplecha type using the recent study by Kikwaya et al. (2011). The average densities reported by Kikwaya et al. (2011) for type A and C meteoroids agree very roughly (i.e. within a factor of 2) with earlier works. While Kikwaya et al. (2011) do not report individual K_B values, Kikwaya Eluo (2011) does. However, Kikwaya Eluo (2011) does not include uncertainties, and so we have recalculated K_B for

Table 1. These meteors appear to have errors in their parameters in appendix A of Kikwaya Eluo (2011) and were therefore excluded from this analysis.

Meteor	Reason for exclusion
20070519040843	Published density disagrees with data provided by coauthors
20070813064415	Orbit is inconsistent with quoted radiant, speed and date
20080911075323	Published density disagrees with data provided by coauthors
20090825060500	Top-of-atmosphere speed appears to have been erroneously copied to $\cos z_R$ field
20090825063641	Geocentric velocity and right ascension have identical values and uncertainties

his set of meteors using the provided trajectory information and including the +0.18 shift in K_B needed for that data set (Kikwaya et al. 2011). Kikwaya et al. (2009) did not report entry angle and this data set is therefore excluded from our K_B plot.

We were able to calculate K_B for the meteors presented by Campbell-Brown et al. (2013) and have included them in our plots for comparison. However, we would like to note that Campbell-Brown et al. (2013) did not systematically survey the available parameter space and therefore their density values may correspond to local, rather than global, extrema in goodness-of-fit; in many cases, the density obtained from the thermal erosion model was substantially different from that obtained using the thermal disruption model.

We calculated K_B values using atmospheric densities from the MSIS 2000 model (Picone et al. 2002) as implemented in the PYGLOW PYTHON package.[1] The latitude and longitude of each meteor were provided by several co-authors of the Kikwaya et al. (2011) and Campbell-Brown et al. (2013) papers; we input this location information, along with meteor heights, into our atmosphere model to obtain local air density values. Uncertainties in speed and starting height were propagated through to uncertainty in K_B, along with an assumed 15 per cent uncertainty in atmospheric density (Hedin 1991; Marcos, Bowman & Sheehan 2006; Stober et al. 2012).

Despite using a different atmosphere model (Kikwaya Eluo 2011 uses MSISE-90), our values are in good agreement with those of Kikwaya. There were a few exceptions, which appear to be due to errors in Kikwaya Eluo (2011) (see Table 1). The results are shown in Fig. 1. Although there appears a slight trend in density with K_B where meteoroids with the lowest K_B values have a smaller range of densities, overall the correlation between the two quantities is weak. Both high and low densities are represented over most of the range of K_B, making K_B a poor proxy for density.

Besides the possible errors listed in Table 1, we noticed that the upper and lower bounds on density are sometimes swapped. In these plots, we used the uncertainties quoted in appendix A of Kikwaya Eluo (2011), which are in agreement with the plots, if not the tables, of Kikwaya et al. (2011).

We are not the first authors to note that measuring K_B may not be an effective way to determine the material properties of meteoroids. Koten et al. (2004) found that for many meteor showers, K_B was a function of meteor magnitude. This indicates that either members of a meteor shower do not have the same material properties or

[1] https://github.com/timduly4/pyglow

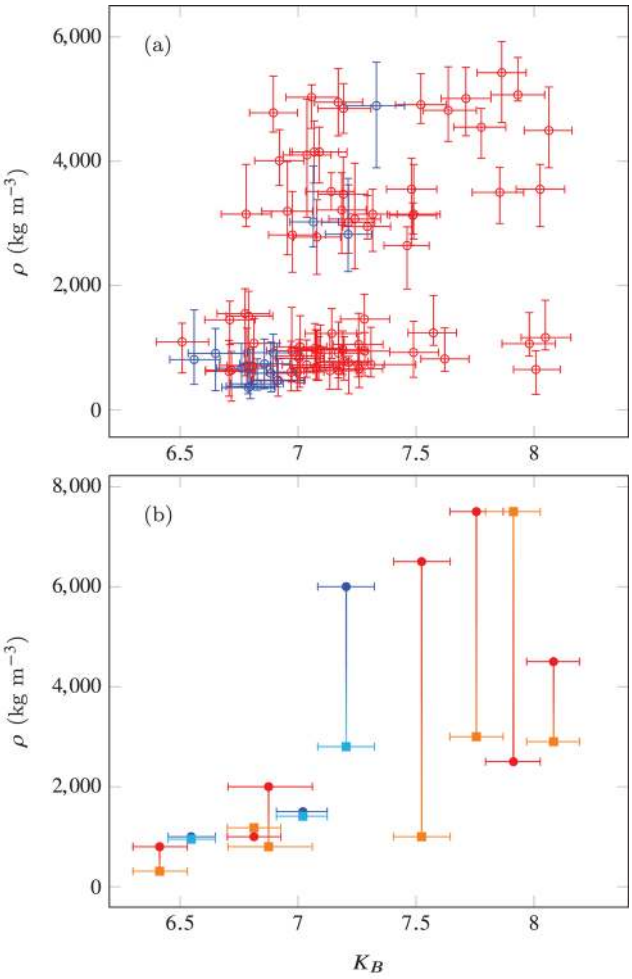

Figure 1. Meteoroid bulk density versus K_B for meteors modelled by (a) Kikwaya et al. (2011) and (b) Campbell-Brown et al. (2013). Sporadic meteors appear in red or red/orange while shower meteors appear in blue or blue/cyan. Uncertainties in start height and speed are converted to uncertainty in K_B and we assume 15 per cent uncertainty in atmospheric density. In (b), red and blue circles mark densities obtained using the thermal disruption model of Campbell-Brown & Koschny (2004) while orange or cyan squares mark densities obtained using the thermal erosion model of Borovička et al. (2007). In many cases, the two models produce highly disparate densities.

that K_B is not an effective probe of these properties. Koten et al. (2004) hypothesized that observers may not be able to detect the true start of ablation. Regardless of the underlying reason, Koten et al. (2004) and Kikwaya et al. (2011) indicate that K_B is likely not a useful density proxy.

4 CORRELATION WITH T_J

Kikwaya et al. (2011) noticed that their modelled densities were correlated with the Tisserand parameter, T_J; we reproduce a version of their plot of density versus the Tisserand parameter in Fig. 2(a). The correlation between the two properties is clearly visible, just as it is in Kikwaya et al. (2011). The meteors appear to be divided into two main populations: one of which corresponds to $T_J \lesssim 2$ and $\rho < 2000$ kg m^{-3}, and the other to $T_J > 2$ and $\rho > 2000$ kg m^{-3}.

This division in density coincides with the division between Halley-type and nearly isotropic comets (HTCs and NICs; for which $T_J < 2$) and Jupiter-family comets (JFCs; for which $2 < T_J < 3$).

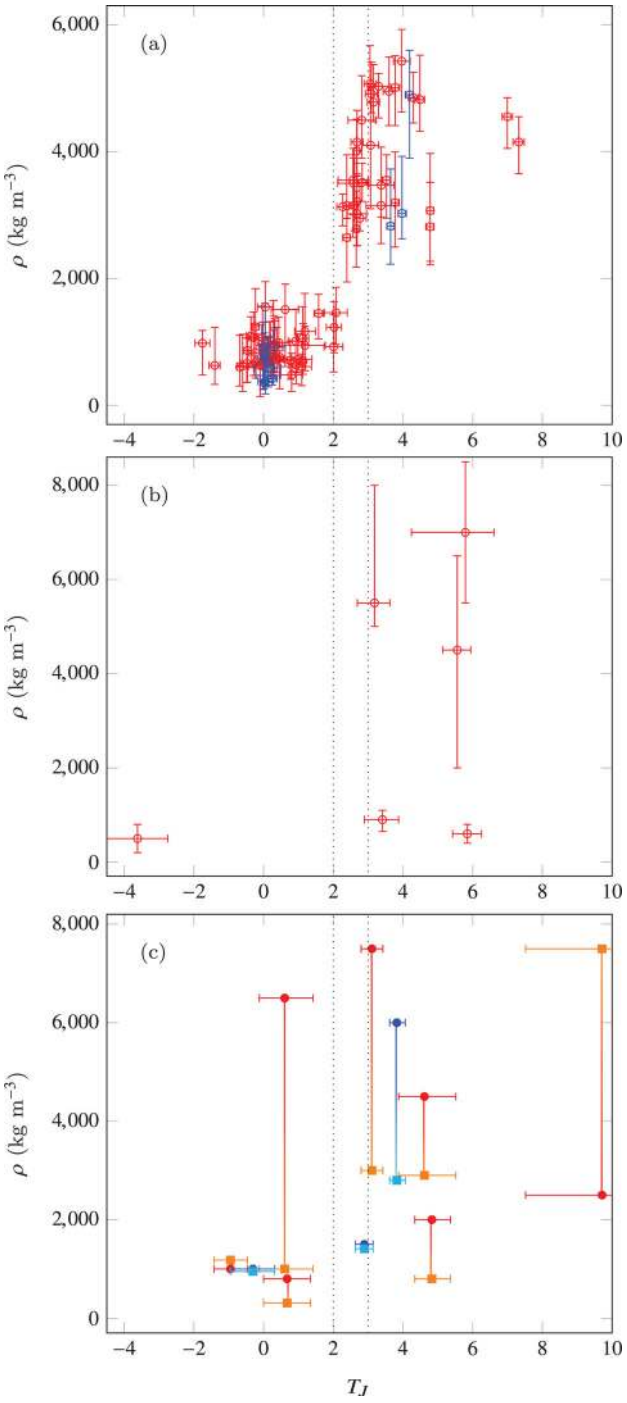

Figure 2. Density versus T_J for meteors modelled by (a) Kikwaya et al. (2011), (b) Kikwaya et al. (2009) and (c) Campbell-Brown et al. (2013). Tisserand parameters were recalculated from each work's reported solar longitudes or dates, geocentric velocities and geocentric radiants; and error bars were added. As in Fig. 1, sporadic meteors appear in red and orange, while shower meteors appear in blue and cyan. In (c), red and blue circles mark densities obtained using the thermal disruption model, while orange and cyan squares mark densities obtained using the thermal erosion model. The dotted lines correspond to the dynamical boundaries of $T_J = 2$ and $T_J = 3$.

However, we see no difference in density between meteoroids with JFC-like orbits and those with asteroid-like orbits ($T_J > 3$). This result is somewhat surprising; one might expect more of a division between meteoroids on asteroid-like orbits and those on comet-like orbits. Yet there appears to be little difference in density between $T_J \sim 2.5$ and $T_J \sim 4$. One possible explanation for this is that JFCs can actually span the $T_J = 3$ boundary (Tancredi 2014). There are hints of a bimodal distribution in density for meteoroids with $T_J \gtrsim 2$, but at this time there are not enough measurements to merit further subdivisions.

The high densities found by Kikwaya et al. (2011) for JFC-like meteoroids are in seeming conflict with Borovička et al. (2007). Borovička et al. obtained a very low density of 300 kg m^{-3} for Draconid meteors, which originate from JFC 21P/Giacobini-Zinner. However, Borovička et al. (2007) also note that the Draconids have unusual behaviour and ablate at higher altitudes than sporadic meteors with comparable speeds. Since no JFC-generated showers are present in the Kikwaya et al. (2009) and Kikwaya et al. (2011) data, it is possible that these studies do not truly conflict. Instead, the discrepancy could represent a true difference in density between young shower meteoroids and old, highly processed sporadic meteoroids.

There are three low-density meteors with Tisserand parameters just over 2 in the Kikwaya et al. (2011) data, however (e.g. meteor 20090825-061542 in table 8 of Kikwaya et al. 2011). The one-sigma uncertainties appear to span the HTC–JFC boundary; to confirm this, we computed 90 per cent confidence intervals in T_J from the uncertainties in perihelion distance, q, eccentricity, e, and inclination, i, published in Kikwaya Eluo (2011). We assumed the uncertainties in these orbital elements followed a normal distribution. Fig. 2 includes these 90 per cent confidence intervals. We find that the two low-density meteoroids near $T_J = 2$ continue to have error bars that span this boundary. We have therefore grouped them with the $T_J < 2$ meteors for the purposes of deriving a density distribution (Section 5).

When we supplement Kikwaya et al. (2011) with meteors from Kikwaya et al. (2009) and Campbell-Brown et al. (2013), the division between the low T_J, low-density group and the high T_J, high-density group is less stark. Kikwaya et al. (2009) obtained low densities for two meteors with $T_J > 3$. Campbell-Brown et al. (2013) similarly obtained low densities for one or two high-T_J meteors and a possible high density for one low-T_J meteor (depending on whether the thermal disruption or thermal erosion model is used). Because Campbell-Brown et al. (2013) did not attempt to find a global chi-square minimum, the significance of these exceptions is unclear. We exclude the Campbell-Brown et al. (2013) data from our analysis in Section 5, but we do include all six data points from Kikwaya et al. (2009).

5 TWO POPULATIONS

Motivated by the correlation between T_J and density reported by Kikwaya et al. (2011), we divide sporadic meteoroids into two groups: (1) those we believe to originate from HTCs or NICs, with Tisserand parameters less than 2, and (2) all other meteoroids. There is no clear benefit of further subdividing these groups. The density distribution of meteoroids with low Tisserand parameters is presented in Fig. 3, and those with high Tisserand parameters appear in Fig. 4.

In constructing our distribution, we use the densities of only sporadic meteors from Kikwaya et al. (2009, 2011). We do not include data from Campbell-Brown et al. (2013) because, as mentioned previously, this later work did not include a systematic search of

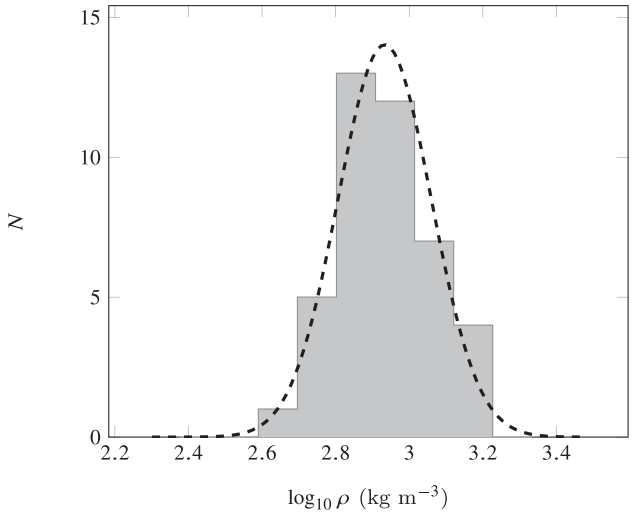

Figure 3. Distribution of bulk densities for sporadic meteoroids with HTC-like orbits, taken from Kikwaya et al. (2009, 2011) (solid grey). These data correspond to 42 meteors with $T_J \lesssim 2$. A normal distribution has been fitted to the data (dashed black line).

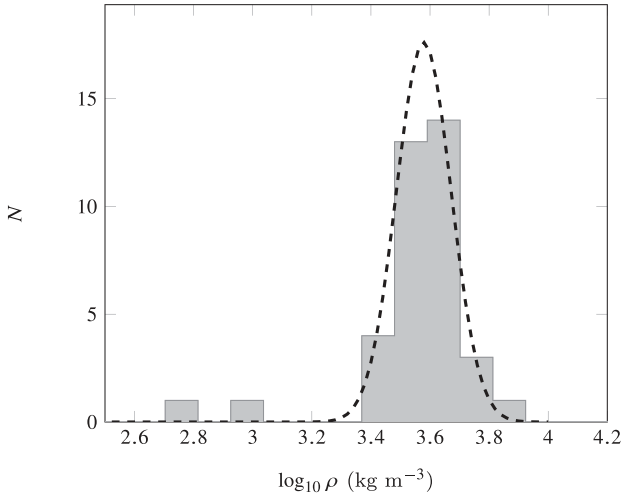

Figure 4. Distribution of bulk densities for sporadic meteoroids with non-HTC-like orbits, taken from Kikwaya et al. (2009, 2011) (solid grey); JFC-like orbits are not separated from asteroidal orbits. These data correspond to 37 meteors with $T_J > 2$. A normal distribution has been fitted to the data (dashed black line). Note the presence of the two low-density meteors from Kikwaya et al. (2009); we find that these outliers do not significantly shift the distribution.

Table 2. Parameters corresponding to the normal fits displayed in Figs 3 and 4. Densities are in kg m^{-3}.

	$(\log \rho)_0$	ρ_0	σ
$T_J \lesssim 2$	2.933(20)	857	0.127(14)
$T_J > 2$	3.579(16)	3792	0.093(12)

parameter space to find the best density value. We fit a normal distribution to the logarithm of the density; the small size of the data set does not justify any more complex distribution function. The parameters of these fits are given in Table 2, and the uncertainties quoted are uncertainties in the fit alone. The probability distributions of individual densities in Kikwaya et al. (2009, 2011) are neither normal nor symmetric, and so a parametric bootstrap was not attempted. Finally, the uncertainties in individually modelled meteoroid densities are not believed to be interrelated, i.e. we do not believe that they are systematically low or high.

We note that the smaller the meteoroid, the more its orbit may have been altered by radiative forces. For very small meteoroids, T_J may no longer resemble that of the parent body. For example, the integration of equations (54) and (55) of Dohnanyi (1978) shows that, for a diameter of 100 μm and a density of 1000 kg m^{-3}, meteoroids ejected from Comet 8P/Tuttle can cross the $T_J = 2$ boundary in less than 80 000 years due to Poynting-Robertson drag. For comparison, Wiegert, Vaubaillon & Campbell-Brown (2009) used a period of 10^5 yr to generate their sporadic model. Similarly, numerical simulations of ejecta from JFCs (Nesvorný et al. 2011) indicate that particles near the low end of the threat regime can drift from a T_J value of 2.9 to 3 or 3.05 in several thousand years (depending on particle size) due to Poynting-Robertson drag (Pokorný, private communication.) This drift is unlikely to be important for the data shown here: the meteors modelled by Kikwaya et al. (2011) are large enough (the smallest has a photometric mass of 7.95×10^{-5} g) that Poynting-Robertson drag is minimal. At 4.41×10^{-5} g, the smallest meteoroid in Kikwaya et al. (2009) is half as massive, but lies nowhere near the $T_J = 2$ boundary. However, we do advise caution against assigning densities to microgram-or-smaller meteoroids based on T_J alone. Fortunately, for dynamical models such as MEM or that of Wiegert et al. (2009), the parent body of all simulated meteoroids is known, and we can therefore apply these density distributions according to the Tisserand parameter of the modelled parent body.

6 IMPLICATIONS FOR THE METEOROID ENVIRONMENT

There are many studies in which meteor astronomers or engineers have assumed a single density value for the entire meteoroid population (including that of the NASA Meteoroid Environment Office: MEM; McNamara et al. 2004). We do not intend to criticize this assumption – reliable meteoroid density measurements have been scarce for many decades – but it can have implications for the derived environment, as we demonstrate in this section.

First, we investigate the effects of density on meteor detectability. Both the brightness of a meteor and the level of ionization it produces, which respectively govern its optical and radar detectability, are proportional to the mass-loss rate from the meteoroid as it ablates: $L \propto dm/dt$ or $q \propto dm/dt$. (The equation for luminosity also includes a deceleration term, but this is typically ignored.) The mass-loss rate for solid-body ablation is given by McKinley (1961) as:

$$\frac{dm}{dt} = -\frac{\Lambda A}{2\xi}\left(\frac{m}{\rho_m}\right)^{2/3}\rho_a v^3, \quad (2)$$

where Λ is the heat transfer coefficient, A is the shape factor, ξ is the energy required to ablate one unit of mass, ρ_a is atmospheric density, ρ_m is the meteoroid bulk density and v is the meteor's observed speed.

Equation (2) indicates that for a given shape factor, ablation energy, heat transfer coefficient, speed, height and mass, a denser meteoroid will be dimmer due to its reduced cross-sectional area. However, a denser meteoroid will retain its mass longer and reach peak ablation at a lower height, where the air density is greater. Fig. 5 shows luminosity versus height for two meteoroids with the same initial mass, speed and entry angle, but different density. The

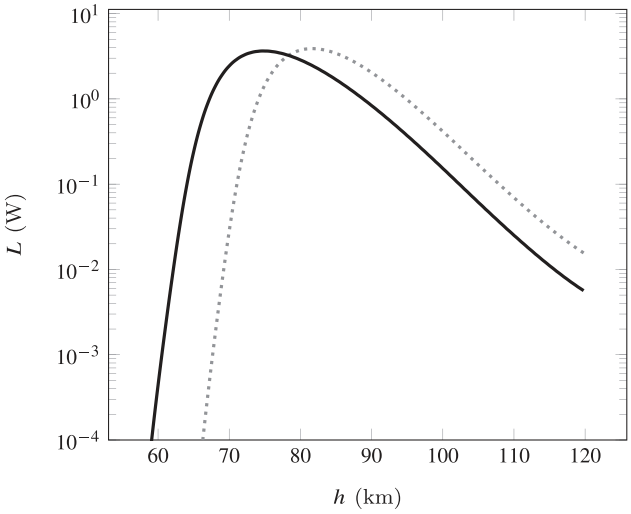

Figure 5. Luminosity corresponding to a 10^{-6} kg meteoroid entering the atmosphere with a speed of 30 km s^{-1} and at an angle of 45°. Two densities were used: 806 (dashed grey line) and 3764 kg m^{-3} (solid black line). The two cases have very similar peak brightnesses. These light curves were computed assuming a constant luminous efficiency of $\tau = 0.7$ per cent.

denser meteoroid reaches peak brightness at a height that is 10 km lower, and the air density compensates for the reduced surface area. The peak brightness for the denser meteoroid is only 10 per cent lower than for the less dense meteoroid. Besides this simple example, we modelled 200 non-fragmenting meteors with a wide range of masses, speeds, zenith angles, and for densities from 1000 to 8000 kg m^{-3}, using the Campbell-Brown & Koschny (2004) model. For typical densities, these simulations showed differences in peak brightness that were typically 0.1 mag or less; an extreme factor of 8 difference in density produced a difference in peak magnitude of less than 1 mag. We therefore conclude that meteoroid detectability is more-or-less insensitive to density.

In our two runs, we have used the same ablation energy, or heat of ablation. The values of ablation energy reported by Kikwaya Eluo (2011) show no correlation with density. However, Borovička et al. (2007) obtained high values of ablation coefficient (which is inversely proportional to ablation energy) for low-density Draconid meteors. Similarly, Stokan (2014) points out that several studies have obtained values of ξ for shower meteors that are lower than the heat of vaporization of stone. If there is some correlation between ξ and density, the relationship between peak brightness and density could differ from what we show here.

In contrast, dense meteoroids are more hazardous to spacecraft. This is apparent in BLEs; the modified Cour–Palais equation for the depth of a hypervelocity impact crater (Hayashida & Robinson 1991) illustrates this dependence:

$$d = 6.58\, m^{19/54} B^{-1/4} \rho_{\rm m}^{4/27} \rho_{\rm t}^{-1/2} (v_{\perp}/c)^{2/3}, \tag{3}$$

where d is crater depth in cm, B is the Brinnell hardness for the target, $\rho_{\rm m}$ is the density of the impactor, $\rho_{\rm t}$ is the density of the target, $v_{\perp}$ is the component of the impactor's velocity normal to the target surface, and c is the speed of sound for the target (cgs units are typically used with BLEs). From equation (3), we see that for a given minimum crater depth $d_{\rm crat}$, and holding all other properties constant, the limiting mass decreases as density increases:

$$m_{\rm crat} \propto \rho_{\rm m}^{-8/19} d_{\rm crat}^{54/19}. \tag{4}$$

If we assume that the cumulative meteoroid flux is inversely proportional to mass, $N(m) \propto m^{-1}$, then the relative contribution of meteoroids of a particular density to the crater flux, as compared to the observed meteor flux, is:

$$N_{\rm crat} = m_{\rm crat}^{-1} \propto \rho_{\rm m}^{8/19}. \tag{5}$$

We now consider the effect this has on our two density populations. The apex source, which constitutes about 30 per cent of meteors detected by CMOR (Campbell-Brown 2008), is thought to derive from HTCs and NICs (Wiegert et al. 2009) and thus corresponds to our low-density population. The helion and antihelion sources, which constitute about 50 per cent of meteors seen by CMOR, are thought to derive primarily from Comet 2P/Encke ($T_{\rm J} = 3.026$) and/or JFCs (Nesvorný et al. 2010), and therefore correspond to our high-density population. The north toroidal source constitutes the remaining 20 per cent; it has been linked to HTCs (Wiegert et al. 2009; Pokorný et al. 2014) and therefore also corresponds to our low-density population. If we assume that the south toroidal source is of a similar strength, then helion and antihelion meteors would constitute 43 per cent of radar-detectable meteors. In comparison, the fraction of nighttime meteors with radiants north of the ecliptic that belong to the antihelion source is 38 per cent. Thus, let us assume that the helion and antihelion sources comprise about 40 per cent of radar-detectable meteors. If we apply equation (5) to the density values in Table 2, we obtain the following cratering ratio:

$$\frac{N_{\rm crat,hel}}{N_{\rm crat}} = \frac{3764^{8/19} 0.4}{3764^{8/19} 0.4 + 806^{8/19} 0.6} = 0.56. \tag{6}$$

In other words, correcting for density alone yields an environment in which the majority of meteoroid impact craters on spacecraft originate from helion and antihelion meteoroids.

The above calculation is crude and intended to demonstrate the impact of a non-uniform density. However, the contribution of the sporadic sources to the spacecraft cratering rate needs to also be corrected for observing biases related to meteor speed, which will further boost the importance of the helion and antihelion sources (Campbell-Brown 2008).

As a final demonstration of the role of density in debiasing observations, we combined our density model with the debiasing method from Moorhead et al. (2017). Instead of correcting the distribution to a constant limiting mass (as described in equation (12) of Moorhead et al. 2017), we correct to a constant limiting crater depth by weighting each individual meteor as follows:

$$w_i = \frac{N(m > m_{{\rm ref},i})}{N(m > m_{\rm lim}(v_i, R_i, h_i, \theta_i, \phi_i))} \tag{7}$$

$$m_{{\rm ref},i} = m_{\rm ref} \left(\frac{\rho_i}{1000 \text{ kg m}^{-3}} \right)^{-8/19} \left(\frac{v_i}{20 \text{ km s}^{-1}} \right)^{-36/19} \tag{8}$$

where v_i, R_i, h_i, θ_i and ϕ_i are the observed velocity, range, height, azimuth and altitude of meteor i. The quantity $m_{\rm lim}$ is the corresponding minimum mass observable by CMOR, and is defined by equation (10) of Moorhead et al. (2017). For each meteor, a density of ρ_i is randomly drawn from the distributions shown in Figs 3 and 4. The quantity $m_{\rm ref}$ is an arbitrary reference mass that we have set to be the median value of $m_{\rm lim}$ for our set of CMOR meteors. Equation (8) is derived from equation (3) and converts $m_{\rm ref}$ to masses that correspond to the same crater depth given variable speed v_i and density ρ_i. We also apply a collecting area correction based on meteor radiant declination using fig. 6 of Campbell-Brown & Jones (2006).

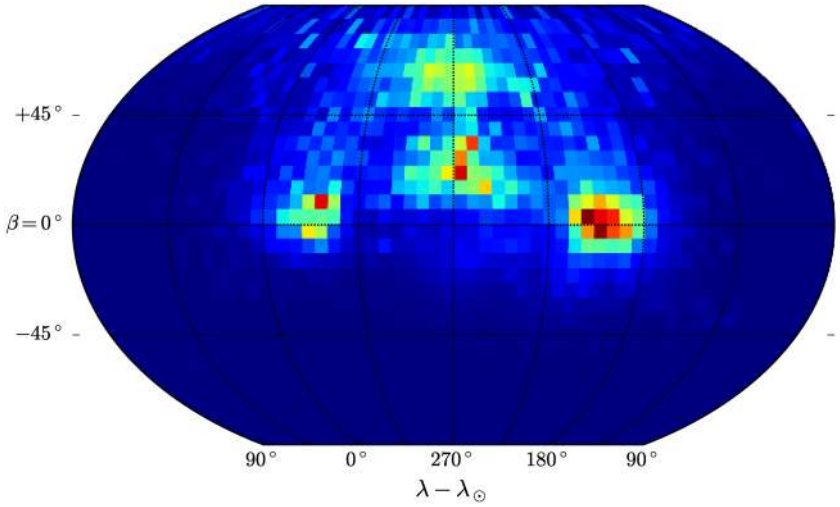

Figure 6. Crater-limited radiant map generated using observations from CMOR. Individual meteors have been weighted to account for velocity debiasing (Moorhead et al. 2017) and density (Section 6 of this paper). The coordinate system used here is Sun-centred ecliptic longitude ($\lambda - \lambda_\odot$) and latitude (β). Note that the helion (near $\lambda - \lambda_\odot = 0^\circ$, $\beta = 0^\circ$) and antihelion sources (near $\lambda - \lambda_\odot = 180^\circ$, $\beta = 0^\circ$) dominate.

Fig. 6 shows the results of debiasing CMOR observations using the density distributions derived in this paper. Because CMOR is unable to detect the southern toroidal source, we will use the nighttime, northern quadrant ($90^\circ < \lambda - \lambda_\odot < 270^\circ$, $\beta > 0$) to compare sporadic source strength. In this quadrant, the antihelion source constitutes 38 per cent of detections; after weighting the data to a constant limiting crater size, it constitutes 75 per cent of craters. Thus, including higher densities for the helion and antihelion source can have significant consequences for both the interpretation of *in situ* data and assessing the risk of meteoroid impacts on Sun-facing spacecraft surfaces.

7 CONCLUSIONS

A bulk density model is needed for accurate meteoroid environment modelling; simultaneously, recent advances in ablation modelling have begun to generate usable constraints on density for individual meteoroids. However, density proxies are needed to extrapolate a global sporadic meteoroid density model from the limited set of modelled meteoroids. We first considered K_B parameter, which has often been used to characterize the material properties of meteoroids, as a proxy for density. However, our investigation shows that little correlation exists between K_B and bulk densities obtained by Kikwaya et al. (2011) and Campbell-Brown et al. (2013). Instead, the correlation between density and the Tisserand parameter reported by Kikwaya et al. (2011) appears to be much more robust.

We therefore propose a two-population density distribution for the meteoroid environment in which each population follows a log-normal distribution (see Table 2). Meteoroids arising from parent bodies with Tisserand parameters below 2, including the apex and toroidal sporadic sources, correspond to the lower-density population, and those arising from all other parent bodies correspond to the higher-density population. We believe this is the most detailed density distribution that is justified by the data available at this point in time. While we acknowledge that Kikwaya Eluo (2011) warns against applying his results to the meteoroid environment as a whole (his sample is biased towards meteors that ablate at low altitudes), the division between low-density, low-T_J meteors and high-density, high-T_J meteors appears quite strong. We see no evidence that he would have been unable to detect, for example, low-density meteors with high T_J values. Until contradictory data appear, we suggest the use of two density distributions that describe meteoroids originating from HTCs and NICs and those originating from other comets and asteroids.

This density distribution is significantly different, yet not entirely inconsistent, with earlier choices and measurements of density. For instance, Grün et al. (1985) assume a constant meteoroid density of 2500 kg m^{-3}. This value lies in the centre of the density values measured by Kikwaya et al. (2011), albeit in a trough between the two distributions. Drew et al. (2004) obtained bulk density values near 1000 kg m^{-3} by applying a non-fragmenting ablation model to meteoroids detected by HPLA (high-power large-aperture) radars. However, their sensitivity to apex meteoroids would certainly bias their results towards low densities. Finally, both high- and low-density particles have been found in comet 67P's ejecta. Comet 67P's classification as a JFC would associate it with the denser of our two populations; however, if the lighter particles are preferentially destroyed, the result could be consistent with our model.

We found that for meteoroids of a given mass, peak brightness is fairly insensitive to meteoroid bulk density. Thus, optical surveys do not require density de-biasing. However, spacecraft damage is more severe for dense meteoroids. This in turn means that spacecraft will experience more damage from helion and antihelion meteoroids. This can alter the interpretation of *in situ* experiments. On a more practical note, meteoroid environment models will need to incorporate this effect in order to accurately assess risk, particularly for elements such as solar panels and heat shields that face towards the helion or antihelion sources.

ACKNOWLEDGEMENTS

This work was supported in part by NASA Cooperative Agreement NNX11AB76A and by the Natural Sciences and Engineering Research Council of Canada. PGB made use of the ShareLaTeX editor in contributing to this work.

REFERENCES

Babadzhanov P. B., 2002, A&A, 384, 317
Bellot Rubio L. R., Martínez González M. J., Ruiz Herrera L., Licandro J., Martínez-Delgado D., Rodríguez-Gil P., Serra-Ricart M., 2002, A&A, 389, 680
Borovička J., 2006, in Daniela L., Sylvio Ferraz M., Angel F. J., eds, Proc. IAU Symp. Vol. 229, Asteroids, Comets, Meteors. Cambridge Univ. Press, Cambridge, p. 249
Borovička J., 2007, in Valsecchi G. B., Vokrouhlický D., Milani A., eds, Proc. IAU Symp. Vol. 236, Near Earth Objects, our Celestial Neighbours: Opportunity and Risk. Cambridge Univ. Press, Cambridge, p. 107
Borovička J., Spurný P., Koten P., 2007, A&A, 473, 661
Brownlee D. et al., 2006, Science, 314, 1711
Campbell-Brown M. D., 2008, Icarus, 196, 144
Campbell-Brown M. D., Jones J., 2006, MNRAS, 367, 709
Campbell-Brown M. D., Koschny D., 2004, A&A, 418, 751
Campbell-Brown M. D., Borovička J., Brown P. G., Stokan E., 2013, A&A, 557, A41
Carry B., 2012, Planet. Space Sci., 73, 98
Ceplecha Z., 1958, Bul. Astron. Inst. Czechoslovakia, 9, 154
Ceplecha Z., 1966a, Bul. Astron. Inst. Czechoslovakia, 17, 96
Ceplecha Z., 1966b, Bul. Astron. Inst. Czechoslovakia, 17, 347
Ceplecha Z., 1967, Smithsonian Contributions Astrophys., 11, 35
Ceplecha Z., 1977, Bul. Astron. Inst. Czechoslovakia, 28, 328
Ceplecha Z., 1988, Bull. Astron. Inst. Czechoslovakia, 39, 221
Ceplecha Z., ReVelle D., 2005, Meteoritics Planet. Sci., 40, 35
Ceplecha Z., Borovička J., Elford W. G., Revelle D. O., Hawkes R. L., Porubčan V., Šimek M., 1998, Space Sci. Rev., 84, 327
Close S., Volz R., Loveland R., Macdonell A., Colestock P., Linscott I., Oppenheim M., 2012, Icarus, 221, 300
Cooke W. J., Moser D. E., 2012, in Gyssens M., Roggemans P., eds, Proc. Int. Meteor Conf. 30th IMC, Sibiu, Romania, 2011. International Meteor Organization, p. 9
D'Hendecourt L. L. S., Lamy P., 1980, Icarus, 43, 350
Dohnanyi J. S., 1978, Particle dynamics. Wiley-Interscience, New York, p. 527
Drew K., 2005, Electronic Thesis and Dissertation Repository
Drew K., Brown P. G., Close S., Durand D., 2004, Earth Moon Planets, 95, 639
Flynn G. J., 1990, in Sharpton V. L., Ryder G., eds, Lunar and Planetary Science Conf. Proc. Vol. 20, Lunar and Planetary Science Conference Proceedings. Lunar and Planetary Institute, Houston, TX, p. 363
Flynn G. J., 1994, Planet. Space Sci., 42, 1151
Flynn G. J., Sutton S. R., 1991, in Ryder G., Sharpton V. L., eds, Lunar and Planetary Science Conf. Proc. Vol. 21, Lunar and Planetary Science Conference Proceedings. Lunar and Planetary Institute, Houston, TX, p. 541
Fulle M. et al., 2015, ApJ, 802, L12
Grün E., Pailer N., Fechtig H., Kissel J., 1980, Planet. Space Science, 28, 333
Grün E., Zook H. A., Fechtig H., Giese R. H., 1985, Icarus, 62, 244
Hayashida K. B., Robinson J. H., 1991, NASA/TM-103565
Hedin A. E., 1991, J. Geophys. Res., 96, 1159
Hornung K. et al., 2016, Planet. Space Science, 133, 63
Jacchia L. G., 1952, A Comparative Analysis of Atmospheric Densities from Meteor Decelerations Observed in Massachusetts and New Mexico. Defense technical information center, Fort Belvoir, VA
Jacchia L. G., Kopal Z., Millman P. M., 1950, ApJ, 111, 104
Kikwaya Eluo J.-B., 2011, Electronic Thesis and Dissertation Repository, Paper 96
Kikwaya J.-B., Campbell-Brown M., Brown P. G., Hawkes R. L., Weryk R. J., 2009, A&A, 497, 851
Kikwaya J.-B., Campbell-Brown M., Brown P. G., 2011, A&A, 530, A113
Kohout T. et al., 2014, Meteoritics Planet. Sci., 49, 1157
Koten P., Borovička J., Spurný P., Betlem H., Evans S., 2004, A&A, 428, 683
Leinert C., Grün E., 1990, in Schewenn R., Marsch E., eds, Physics of the Inner Heliosphere I1. Springer-Verlag, Berlin, p. 207
Levin B. I., 1956, Fizicheskaya teoriya meteorov i meteornoe veshchestro v Solnechnoi sisteme (Physical Theory of Meteors and Meteoric Matter in the Solar system). Akademie-Verlag, Berlin
McKinley D. W. R., 1961, Meteor Science and Engineering. McGraw-Hill, New York
McNamara H., Jones J., Kauffman B., Suggs R., Cooke W., Smith S., 2004, Earth Moon Planet., 95, 123
Marcos F. A., Bowman B. R., Sheehan R. E., 2006, AIAA/AAS Astrodynamics Specialist Conference and Exhibit. American Institute of Aeronautics and Astronautics (AIAA), Reston, Virginia
Messenger S., Nakamura-Messenger K., Keller L. P., Clemett S. J., 2015, Meteoritics Planet. Sci., 50, 1468
Moorhead A. V., Brown P. G., Campbell-Brown M. D., Heynen D., Cooke W. J., 2017, Planet. Space Sci., 143, 209
Mukai T., Fechtig H., 1983, Planet. Space Sci., 31, 655
Nesvorný D., Jenniskens P., Levison H. F., Bottke W. F., Vokrouhlický D., Gounelle M., 2010, ApJ, 713, 816
Nesvorný D., Janches D., Vokrouhlický D., Pokorný P., Bottke W. F., Jenniskens P., 2011, ApJ, 743, 129
Opik E. J., 1958, Physics of Meteor Flight in the Atmosphere. Interscience Publishers, New York
Picone J. M., Hedin A. E., Drob D. P., Aikin A. C., 2002, J. Geophys. Res. (Space Phys.), 107, 1468
Pokorný P., Vokrouhlický D., Nesvorný D., Campbell-Brown M., Brown P., 2014, ApJ, 789, 25
Revelle D. O., 1983, Meteoritics, 18, 386
Revelle D. O., 2001, in Warmbein B., ed., ESA Special Publication Vol. 495, Meteoroids 2001 Conference. p. 513
Stober G., Jacobi C., Matthias V., Hoffmann P., Gerding M., 2012, J. Atmospheric Solar-Terrestrial Phys., 74, 55
Stokan E., 2014, Electronic Thesis and Dissertation Repository, Paper 2581
Tancredi G., 2014, Icarus, 234, 66
Wiegert P., Vaubaillon J., Campbell-Brown M., 2009, Icarus, 201, 295

This paper has been typeset from a TEX/LATEX file prepared by the author.